



# Seasonal influence on Post-Fire Debris Flow likelihood after the 2020 Lake Fire

Jeng-Hann Chong<sup>1</sup>, Adit Ghosh<sup>2</sup>, Brandon T. Page<sup>3</sup>, Gregory Jesmok<sup>4</sup>, Denise V. Berg<sup>4</sup>, Marlene Lopez<sup>4</sup>, Deepshikha Upadhyay<sup>5</sup>, David J. Stone<sup>6</sup>, Scott C. Hauswirth<sup>4</sup>, Eric O. Lindsey<sup>1</sup>, Louis A. Scuderi<sup>1</sup>

<sup>1</sup>University of New Mexico, Albuquerque, 87107, U.S. <sup>2</sup>University of Southern California, Los Angeles, 90089 <sup>3</sup>Dudek, 225 S Lake Ave, Suite 225, Pasadena, CA 91101

California State University Northridge, Northridge, 91330
 University of California, Los Angeles, Los Angeles, 90095
 Environmental Resources Management Inc., 1050 SW 6th Ave Suite 1650, Portland, OR 97204

Correspondence to: Jeng-Hann Chong (<u>chongjh11@unm.edu</u>)

https://doi.org/10.5194/egusphere-2025-4671 Preprint. Discussion started: 15 October 2025 © Author(s) 2025. CC BY 4.0 License.



20

25

30

35

40

45

50



#### **Abstract**

The increasing severity of wildfires in Western North America is widely hypothesized to lead to an increased likelihood of post-fire debris flows (PFDF), specifically those triggered by high-intensity rain. PFDF likelihoods are highest in the first year and tend to decrease over time. However, it is not well understood how seasonal variation affects the PFDFs initiation in the years following a fire. Here, we monitored the changes in PFDF likelihood of the 2020 Lake Fire in Southern California over a span of four years using field and satellite observations, together with numerical modeling for a subset of drainage basins. We found that unsaturated hydraulic conductivity increased by an order of magnitude during the dry season as compared to the wet season, significantly reducing the PFDF likelihood. Our simulations show that vegetation cover has a smaller impact on PFDF likelihood as compared to hydraulic conductivity or grain size. This study helps clarify the impacts of hydraulic conductivity, grain size, and vegetation on PFDF due to seasonal variation in these parameters for four years after the fire. We suggest that field measurements and modeling approaches should consider how different climatic and seasonal patterns could influence PFDF several years after fires.

#### 1. Introduction

Wildfires have increased in size and severity in recent years, especially in the western United States (Abatzoglou and Williams, 2016; Singleton et al., 2019). Wildfires significantly alter the landscape by increasing overland flow, which ultimately produces runoff-generated post-fire debris flows (PFDF) in steep basins when the infiltration rate capacity is overwhelmed by rainfall intensity (Kean et al., 2011; Kean et al., 2016). PFDF likelihood is generally exacerbated in areas with high-intensity fires where vegetation canopy interception is significantly reduced, topsoil hydrophobicity is increased (Granged et al., 2011; Nyman et al., 2014; Robichaud et al., 2016), and hydraulic roughness is reduced (e.g., Stoff et al., 2015; Hoch et al., 2021).

Runoff-generated debris flows are considered water-dominated flows that can include a wide range of sediment sizes (Kean et al., 2019), with initiation points varying significantly between watersheds (DeGraff et al., 2015; McGuire et al., 2017). The rainfall intensity-duration (ID) threshold defines the rainfall needed over a set duration that leads to triggering of PFDF (Staley et al., 2013; Staley et al., 2017). Rainfall ID threshold is lowest in the first year for runoff-generated debris flows, regardless of the rainfall regional regimes (DeGraff et al., 2015; Hoch et al., 2021; McGuire et al., 2021a). While the rainfall ID threshold increases over time, runoff-generated debris flows can still be triggered up to 10 years after the fire, especially in extreme precipitation events (DeGraff et al., 2015; Tillery and Rengers, 2020).

Estimating accurate rainfall ID threshold for a large area can be challenging using generalized parameters, but we can attribute several parameter such as soil infiltration capacity, median grain size, and canopy interception that contribute to the yearly changes of PFDF likelihood in the southwestern United States (Ebel and Martin, 2017; Tillery and Rengers, 2020; McGuire et al., 2021a; Hoch et al., 2021; Gorr et al., 2023). Recent studies have shown that seasonal variations in the first two years post-fire can alter the rainfall ID threshold (Gorr et al., 2023; Martinez et al., 2025). However, it is still unclear how seasonal variations greater than four years after the fire can influence the PFDF likelihood.

60



70



In this study, we track the changes in rainfall ID threshold of five relatively high burn severity basins affected by the 2020 Lake Fire, focusing on understanding how seasonal variation influences PFDF. We use data collected from three separate field surveys, during the first year, during a dry and wet month in the fourth year, along with high-resolution, high-repeat satellite imagery and field measurements to estimate the PFDF likelihood immediately after the fire and four years after the fire, in both wet and dry seasons. We show that the rainfall ID threshold remains highly variable depending on seasonal changes in the soil hydraulic conductivity several years after the fire. This work shows the importance of better characterizing seasonal influences on the generation of post-fire debris flows in different climates and regions.

## 2. Study area

The 2020 Lake Fire was the second-largest fire of the year for Los Angeles County, with an estimated burned area of ~125.4 sq. km (USGS Landslide Hazard Program, 2020). US Burned Area Emergency Response (BAER) reports that the area of unburned and very low burn severity 75 was ~7% (117.5 sq km), low burn intensity was ~21% (26.7 sq km), moderate burn severity was ~53% (67.5 sq km), and high burn severity was ~18% (23.1 sq km) (USDA Forest Service, 2020) (Figure 1). We selected five northwest-facing (Basin A to E), moderate-to-high burn severity basins with a high likelihood of debris flow (80-100%) at a peak 15-minute rainfall intensity of 24 mm/hr (USGS Landslide Hazard Program, 2020) (Figure 1). The basins are in the 80 southern region of the burned perimeter, along Lake Hughes Road, with a mean slope of 34 degrees, and with a similar Late Cretaceous lithology of quartz diorite (Valencia et al., 2022). The fire burned within a largely unpopulated portion of the Angeles National Forest, with the overall land cover in the five basins exhibiting a mix of shrubs, deciduous forest, evergreen forest, and mixed forest, including bigcone Douglas fir (Pseudotsuga macrocarpa), oak, and gray pine (Figure 3) (Yang et al., 2018).

#### 3. Methods

### 3.1 Field sampling and observation

90 We selected five basins with the highest probability (relatively high burn severity) for debris flow in all rain intensities as predicted by the USGS Landslide Hazard Program. Field measurements were collected three months after the fire (Year 0), 45 months (wet season of Year 4), and 50 months (dry season of Year 4). We collected field samples at basin outlets for grain size analysis, due to the difficulty of accessing the basin interiors and assuming most eroded sediment passes through the main channel (Santi et al., 2008) (Figure 2). We measured 95 unsaturated soil hydraulic conductivity using a mini disk infiltrometer adjacent to our soil samples. However, we were only able to measure unsaturated hydraulic conductivity for the second and third field surveys in Year 4 due to the lack of instruments and access. For Year 0, we assumed the hydraulic conductivity of 10 mm/hr to be closely related to the Fish Fire in the 100 adjacent San Gabriel Mountains with no vegetation cover at (McGuire et al., 2021a). Canopy throughfall coefficient was defined as the open space calculated by subtracting the vegetation cover from 1 (100%).

## 3.2 Precipitation record

Rainfall intensity was calculated using the precipitation record obtained from the Los Angeles Department of Public Works (LADPW) Elizabeth Lake monitoring site, 1 mile southeast of the



125

130



area of interest (34.6083, -118.5594). The overall rainfall recorded for the first, second, third, and fourth years was 127.5 mm, 404.1 mm, 1329 mm, and 693.7 mm, respectively. There was a cumulative rainfall of 25.4 mm before the first survey in December 2020, with a maximum 15-minute duration (I<sub>15</sub>) of ~1 mm/hr. The highest rain intensity during the first year was I<sub>15</sub>~13 mm/yr, while from Years 2-4 there were 12 days where it exceeded the 15-minute duration threshold, of which 4 days exceeded I<sub>15</sub> = 20 mm/hr, but none exceeded I<sub>15</sub> = 25 mm/hr (**Table S7**; **Figure S2**).

# 3.3 Differenced Normalized Difference Vegetation Index (NDVI)

We estimated the vegetation changes using high-resolution satellite imagery from pre-fire to the fourth year. We acquired PlanetScope (3 meters) images and calculated the Normalized Difference Vegetation Index (NDVI) (Equation 1) within the basins and estimated the differences between pre- and post-NDVI (dNDVI) to estimate the vegetation changes and possible soil mobilization (i.e., debris flows) (Equation 2).

We applied several selection criteria for PlanetScope imagery, including cloud-free within the area of interest, high solar elevation angle (45°-90°) to reduce shadow artifacts, and interoperable with image products from Sentinel-2 (PSB.SD). PlanetScope images consist of 8 bands: Redsixth band, Green-fourth band, Blue-third band, and Near-infrared-eighth band. We calculated NDVI for each image in QGIS's *raster calculator* using the following equation (Carlson and Ripley, 1997):

$$\frac{NIR-Red}{NIR+Red} \tag{1}$$

Where Near-Infrared (NIR) is the eighth band and Red is the sixth band. The NDVI values range between -1 to 1.

Positive NDVI values indicate greener or healthier vegetation, whereas lower or negative NDVI values show less healthy vegetation, bare soil, snow, or water (e.g., Dye and Tucker, 2003). To distinguish areas with landscape change and vegetation recovery between the years, we estimate Differenced Normalized Difference Vegetation Index (dNDVI) between two dates of interest. Pixels with vegetation loss or exposed bare ground exhibit lower dNDVI values, whereas vegetation growth or cover is represented by higher dNDVI values. Although it is difficult to distinguish debris flows and flood events solely from satellite imagery, affected areas from sediment accumulation or high erosion could still show lower dNDVI values (<0) due to the lack of vegetation or exposed soil. The use of dNDVI is similar to the dNBR (differenced normalized burn ratio), where Landsat's mid-infrared band is used (Miller and Thode, 2007).

$$dNDVI = postNDVI - preNDVI$$
 (2)

Where dNDVI represents the difference in Normalized Differences Vegetation Index.

We acquired a total of 61 monthly images from August 2020 (including 3 months before the fire) to September 2024, conforming to the aforementioned criteria (**Table S1**). For simplicity, we compare the yearly changes of dNDVI to estimate vegetation cover for our model input while qualitatively tracking the vegetation recovery and loss (**Table 1**). Our yearly dNDVI images start





and end in either August or September to align with the fire's conclusion in September 2020. We also processed dNDVI between our two surveys in 2024 (**Figure 4**) and defined the observation period leading up to our field surveys: Year 4-Wet spans September 2023 to April 2024, and Year 4-Dry spans April 2024 to September 2024.

#### 3.4 Numerical modeling inputs

We use a slope-dependent dimensionless-discharge numerical model to estimate post-fire debris flow initiation. This model estimates the rainfall ID threshold needed to trigger runoff-generated debris flows using infiltration, interception, runoff, and topography (Rengers et al., 2016b; Tang et al., 2019a; McGuire and Youberg, 2019). Here, we estimate the rainfall ID thresholds that are needed to trigger runoff-generated debris for all our basins for Year 0 (immediately after fire), Year 1, Year 4 (Wet), and Year 4 (Dry). We used a 1-m bare-Earth DEM acquired by the USGS 3DEP lidar program before the fire (last accessed December 2020 from opentopography.org).

Our simulations use an idealized rainfall intensity shaped like a Gaussian function at different intensities (I<sub>15</sub>): 15 mm/hr, 20 mm/hr, and 30 mm/hr, which aligns with the rain intensities recorded at the Elizabeth Lake rain gauge with a max 5-year recurrence interval for I<sub>15</sub> = 30 mm/hr (NOAA, last accessed July 2025). Our highest simulated rain intensity is sufficient given that most PFDFs in the southwest US are triggered during rain events with recurrence intervals less than 2 years (Staley et al., 2020). In our simulations, we input the parameters (i.e., grain sizes, hydraulic conductivity, and vegetation cover) from our field and satellite observations to estimate the rainfall threshold needed to trigger runoff-generated debris flows for all four basins.

A complete list of input parameters for our models can be found in **Table 2**.

We estimated vegetation cover using dNDVI from satellite imagery by calculating the fraction of pixels with dNDVI values greater than 0 within a basin are classified as vegetated (**Table 2**). Immediately after the fire (Year 0), we assumed a fractional vegetation cover of 0. For Year 1, vegetation cover was estimated using dNDVI. For Year 4, we estimated the dNDVI of the wet month survey using imagery between 12<sup>th</sup> September 2023 and 21<sup>st</sup> April 2024, and the dry month survey between 21<sup>st</sup> April 2024 and 27<sup>th</sup> September 2024 (between the second and third field survey).

In Year 1, we assumed that only vegetation cover changed during that period, while maintaining other parameters the same from Year 0. Grain size distributions (d<sub>50</sub> and d<sub>84</sub>) were measured from all three field surveys. Hydraulic conductivity measurements were only available from the final two surveys (wet and dry months in 2024). For Year 0 and Year 1, we assumed a hydraulic conductivity of 10 mm/hr from nearby fires in the San Gabriel Mountains (Rengers et al., 2019;
 Hoch et al., 2021). We set a suction head of 0.01 m, an initial volumetric soil moisture content of 0.1, and a lower end member of a volumetric soil moisture at saturation of 0.3 as observed from nearby fires (Tang et al., 2019b; Hoch et al., 2021; Carsel and Parrish, 1988).

#### 4. Results

180

195

#### 4.1 Postfire recovery surveys

Our dNDVI shows the burn perimeter outlined clearly by the negative dNDVI (loss of vegetation) immediately after the fire (**Figure 3a**). The highest negative dNDVI is within the lower elevations of Basin C, in the larger basin across from Basin C, and along the portions of





the river. These negative dNDVI changes could indicate significant vegetation loss, increased soil exposure, or sediment deposition, such as from a culvert transporting sediments across Basin C. The highest negative dNDVI from our higher spatial resolution process is similar to locations with the high burn severity from the US BAER, which uses either Landsat or Sentinel-1 to estimate their burn severity. Immediately after the fire, our simulations show that Basins A, B, D, and E require at least I<sub>15</sub> = 30 mm/hr to trigger runoff-generated debris flows (**Figure 5**), although there were no significant high-intensity rainfall events recorded during that time (**Figure S3**). We do not report Basin C as we did not have sufficient data collected in the subsequent years

In Year 1, the precipitation record shows a lack of significant cumulative precipitation and rain intensity (max I<sub>15</sub> = 13 mm/hr) (**Figure S2**). The effects of a low cumulative precipitation can be seen with the low positive dNDVI that indicates low vegetation recovery across the burn scar (**Figure 3b**) (**Table 2**). The majority of positive dNDVI values are located along the river and within some of the basins (i.e., Basin A, Basin C, Basin E). We also observe a positive dNDVI region downstream of Basin A along the slopes, where we suspect that these are rapidly growing vegetation (i.e., grasses). Our simulations show similar results as compared to Year 0 when we only increased the vegetation cover based on our dNDVI. Similarly, we assumed no runoffgenerated debris flow occurred during this period due to the lack of high-intensity rainfall from our simulations (**Figure 5**).

220 In Year 2, there is an increase in areas of negative dNDVI along the river, possibly indicating sediment deposition or exposure of soil. We suspect that the negative dNDVI along the river is unlikely to be vegetation die-off due to the surrounding increase of positive dNDVI during the same period (Figure 3c). We also identified negative dNDVI values southeast of our basins on the slope face, outside of the burn perimeter, but we could not discern if they indicate erosional 225 or depositional features. We propose that the negative dNDVI along the river is likely mostly sediment deposition, given that we recorded days with higher rain intensities (March 2022 exceeded 20 mm/hr) that could trigger debris flows either within our basins or upstream (outside our study area). In Year 3, we observed a greater positive dNDVI along the river than the basins. This likely indicates increased vegetation growth by the river than on the slopes due to increased 230 precipitation, as seen in the precipitation record (Figure 3d). There were seven events exceeding 15 mm/hr within this period, with three exceeding 20 mm/hr (Figure S2). We are unable to verify if the negative dNDVI within some areas of the hillslope and by the river represents sediment erosion or debris flows that occurred and deposited due to the road inaccessibility to the sites (Figures 3c & 3d).

In Year 4, from September 2023 to April 2024, both field observation and satellite imagery from April 2024 show increased positive dNDVI along the basins and negative dNDVI along the river (Figures 3e & 4). We posit that the positive dNDVI is indicative of the growth of dense shrubs and grasses due to prior increased precipitation, while negative dNDVI values indicate sediment deposition or removal from rain events, vegetation change, or an increase in water level. Between April 2024 and September 2024 (Figure 4), we observed significant vegetation change with basin slopes exhibiting negative dNDVI values and areas along the river exhibiting positive dNDVI, possibly showing different vegetation responding to the seasonal changes (Figure 2e & 2f). Measured hydraulic conductivity increased by almost an order of magnitude except for Basin



255

260

265

290



A (**Table 2**). Grain sizes were comparable between April 2024 and September 2024 across all basins but were generally reduced compared to the first survey in 2020 (**Table 2**).

Our simulations show that all basins during the wet month of Year 4 could trigger debris flows at  $I_{15} = 30$  mm/hr, except Basin D, where they could be triggered at 20 mm/hr (**Table 3**, **Figure S2**), for which we identified two rain events with very closely matching rain intensity (4<sup>th</sup> and 7<sup>th</sup> February 2024). We do observe an increase in areas of negative dNDVI along the river while the basins have mostly positive dNDVI (**Figure S4d**). During the dry months of Year 4, all basins except for Basin A were unlikely to trigger debris flows, and possibly had no surface runoff even at  $I_{15} = 30$  mm/hr. In contrast, Basin A could potentially trigger debris flows at  $I_{15} = 20$  mm/hr.

#### 5. Discussion

### 5.1. Evolution of the landscape and post-fire debris flow likelihood

Our simulations informed by the three field surveys suggest that most basins require at least I<sub>15</sub>= 30 mm/hr to trigger debris flows. Observations from nearby fires in Southern California have been shown to have a wide range of triggering rain intensity (I<sub>15</sub>) in the first year, ranging from less than 10 mm/hr (Cannon et al., 2008; Hoch et al., 2021) to 30 mm/hr (McGuire et al., 2020). In the subsequent years, the intensity needed to trigger debris flows increased by at least a factor of two (McGuire et al., 2020; McGuire et al., 2021a; Hoch et al., 2021). Our simulations show that at least I<sub>15</sub> = 80 mm/hr is needed to trigger PFDFs in the dry season for basins B to D, which correspond to the I<sub>15</sub> associated with a 100- to 200-year precipitation event (NOAA, last accessed July 2025). The highly variable rainfall ID threshold among adjacent basins within the burn perimeter could be due to the basin topography (Staley et al., 2013).

Simulations of the Year 4 wet season show higher debris flow triggering likelihoods despite 270 having more vegetation cover than Year 0, contrary to other fires (e.g., DeGraff et al., 2015) (Figure 5). We suspect the main causes of this increase in PFDF likelihood are due to the relatively lower hydraulic conductivity (wetter soil) measured in the wet months and finer grain sizes as compared to the first survey (Figure 5; Table 2 & 3). Similarly, lower measured hydraulic conductivity in Basin A during the dry months also contributes to a higher PFDF 275 likelihood shown in our simulations. Our field observations revealed that moist and wetter soil around Basin A during dry months could have lowered the hydraulic conductivity. For the other basins with measured high hydraulic conductivity in the dry months, the drier conditions can promote the opening of macropore fractures in the soil, allowing for a significant increase in hydraulic conductivity by several factors (Nyman et al., 2014; Perkins et al., 2022; Martinez et al., 2025). Martinez et al., (2025) estimated a ~5-fold increase in mean field hydraulic 280 conductivity in the Contreras Fire in Arizona between the first dry and wet seasons. By comparison, our highest measured hydraulic conductivity shows several orders of magnitude variation in seasonal variability and is approximately 2 to 4 times greater than values reported by Martinez et al., (2025). 285

Hydraulic conductivity measurements can be used effectively immediately after fires across multiple basins with similar burn severity (Rengers et al., 2019). However, it is also important to consider both regional climate and the timing of field surveys as monsoons, droughts, and seasonal variability that can influence soil properties (Cannon et al., 2001; DeGraff et al., 2015; Ebel et al., 2022; Thomas et al., 2023; Gorr et al., 2023; Gorr et al., 2024; McGuire et al., 2024;





Martinez et al., 2025). The large variability in hydraulic conductivity between seasons in the first two years suggests the importance of considering seasonal influence in estimating longer-term PFDF likelihoods (Martinez et al., 2025) and we show that the effects of seasonal variability can continue in the fourth year.

295

300

Although vegetation cover can play a role in debris flow initiation (Rengers et al., 2016a; Tillery and Rengers, 2020; McGuire and Youberg, 2020; McGuire et al., 2021a; McGuire et al., 2024), our simulations suggest a minimal influence on PFDF likelihood as compared to grain size and hydraulic conductivity. For example, when we maintain all parameters from Year 0 but include higher vegetation cover in Year 1, the rainfall ID threshold shows little difference in all the basins (**Figure 5**), which implies that vegetation cover does not significantly change the likelihood of debris flow. This contrasts with results from the nearby San Gabriel Mountains, where vegetation and hydraulic conductivity have been implicated as contributing equally to triggering debris flows (McGuire et al., 2021a).

305

310

Despite a significant increase in vegetation cover in our dNDVI after Year 2 due to precipitation (Keeley et al., 2005; Horn and St. Clair, 2017) (**Figure 3; Figure S2**), a full vegetation recovery does not necessarily inhibit triggering of PFDF if other conditions enable it (Garber et al., 2023). We note, however, that vegetation cover and hydraulic conductivity are not necessarily independent of each other (Atchley and Maxwell, 2011) – increased vegetation cover increases evapotranspiration demand, resulting in faster drying of soils (Zhang et al., 2001), and potentially a more rapid return to higher hydraulic conductivity states. Our temporal sampling is insufficient to resolve this phenomenon but would be an important avenue for future study.

315

320

325

Median grain size from the first survey was larger than the subsequent two surveys in the same year but did not show great median grain size variability between seasons (**Table 2**). Grain size variability over time has been observed in other fires where grain size can be consistent or increase during the recovery period (e.g., Hoch et al., 2021). It is possible that our point source grain size measurement is not sufficient to represent the change in the entire basin, despite prior work suggesting that basin outlets capture representative grain sizes for the basin (Santi et al., 2008). Another explanation is that repeated rainfall has removed coarser material and revealed a finer baseline grain size that could represent the hillslope materials (Kean et al., 2019), as shown by consistent grain sizes across the wet and dry seasons. Since we collected samples at the basin outlets, any existing debris flow would leave behind a higher concentration of finer materials in the body (center) as it exited the basin outlet (Iverson et al., 2010). Alternatively, we could be observing deposited finer sediments that are easier to mobilize (Lamb et al., 2008), burying the coarser sediments. In any case, the observed variation in grain sizes was not the most significant factor affecting PFDF in our results (**Figure 5**). Future work is needed to better characterize true basin-scale grain size variability over the recovery period.

330

335

**5.2** Sensitivity tests between hydraulic conductivity, grain size, and vegetation cover Higher rain intensities lead to an increase in PFDF likelihood. Studies have also shown that greater rainfall intensities are required to trigger debris flows in the subsequent years after a fire (Caine, 1980; Cannon et al., 2008; Kean et al., 2011; Staley et al., 2013; Tang et al., 2019a; Hoch et al., 2021; Thomas et al., 2021; Thomas et al., 2023). We performed a sensitivity test for each



360

375

380



basin at different rain intensities to isolate the effects of hydraulic conductivity, grain size, and vegetation cover on post-fire debris flow triggers (Figure 6; Table 4).

A major difference between the wet and dry seasons from our field surveys is the hydraulic 340 conductivity and vegetation cover (Figures 6 & 7). The significant increase in our measured hydraulic conductivity plays a strong role in changing the PFDF likelihood despite having an increase in vegetation cover (Figure 6), similar to our simulation results. The sensitivity tests indicate that different parameters have a varying degree of influence on the post-fire debris flow. For instance, Basins B and D show that  $I_{15} = 30$  mm/hr will trigger a significant PFDF for a number of slopes when the grain sizes are reduced by 50%, whereas Basin E is less affected 345 (Figure 6). These results are also sensitive to changes in the magnitude of hydraulic conductivity. For example, if the hydraulic conductivity increases by an order of magnitude or more, as seen in our field observation from the wet to dry season, we expect the hydraulic conductivity will play a stronger role than the grain size. We suspect that the hydraulic 350 conductivity has a greater impact than grain sizes when comparing seasonal impacts, as it is less likely for grain sizes to have such large variability in a short amount of time (Hoch et al., 2021).

While hydraulic conductivity recovery has been shown to increase monotonically to pre-fire levels (Ebel and Martin, 2017), our observations suggest a potentially non-monotonic relationship of hydraulic conductivity despite tracking seasonal variation for only a year. Such non-monotonic changes have been observed in fires in the southwest United States and could have a significant impact in inhibiting or promoting post-fire debris flows (Hoch et al., 2021; Garber et al., 2023; McGuire et al., 2024; Martinez et al., 2025). Despite needing a higher temporal resolution to capture the seasonal signal of hydraulic conductivity, we suggest that it is important to account for seasonal variation when estimating the PFDF likelihood. We suspect the variability in rainfall patterns could also influence the triggering of debris flows (Thomas et al., 2021).

Our sensitivity test on vegetation cover also shows little to no change in the PFDF likelihood between a full and no vegetation cover within basins, assuming soil properties remain constant (Figure 6). Vegetation cover could have a lower impact due to saturation in the presence of high-intensity rain (Hoch et al., 2021), with vegetation playing a stronger role in controlling debris flow volumes than initiation (McGuire et al., 2021b). We also note that satellite-derived vegetation cover does not represent understory density and surface roughness, and canopy interception can vary depending on the vegetation type (Zhao et al., 2019).

Overall, our study suggests that for our study area basins, the combination of lower hydraulic conductivity and finer grain sizes has the strongest impact on triggering runoff-generated debris flows relative to vegetation cover.

#### 5.3 Applicability of high-resolution imagery to estimate vegetation cover

We demonstrated that PlanetScope's high-resolution and high repeat times can successfully track vegetation change and complement field observation, despite challenges in standardizing the images due to low consistency in orbit and imagery acquisition time. Ground cover surveys and Leaf Area Index (LAI) can estimate vegetation cover and vegetation recovery over time but are limited to basins that are accessible or larger to not be affected by the coarse spatial resolution



390

395

400



from satellites such as Sentinel-2 (10 to 30 meters) and MODIS (500 meters) (Rutter et al., 1975; Hoch et al., 2021; Garber et al., 2023). PlanetScope-derived dNDVI can further distinguish between burned and unburned areas even two years post-fire, showing comparable capabilities as LAI measurements in other fire studies (Garber et al., 2023) (**Figures 2 & 3**).

We suggest that the strong seasonal vegetation signal observed between the drier and wetter months four years after the fire is due to the transition from perennial shrubs to annual grasses (**Figures 4 & 7**). This vegetation transition has been observed in other fires in the southwest United States and has the potential to increase fire hazard due to rapid drying (e.g., Keeley et al., 2005; Horn and St. Clair, 2017; Underwood et al., 2021; Thomas et al., 2021) (**Figure 2**). Further research is needed to determine the persistence of large seasonal pattern variations and whether they will return to pre-fire levels, with some studies suggesting recovery may take more than a decade (Bright et al., 2019) (**Figure 7**).

We observed that some trees survived in our post-fire field surveys despite the high burn severity as reported in US BAER and our dNDVI. This could indicate that the satellite-derived products are showing changes from either burned or drying out of leaves during the fire. Our dNDVI might not be able to fully represent Manning's roughness on channels or hillslopes, and more work is needed to validate the best practices of using dNDVI for constraining Manning's roughness. For example, we identified grasses and shrubs that show similar dNDVI values as trees with green leaves but no undergrowth. This suggests that even higher resolution satellite imagery is required to quantify vegetation density.

Additional method validation through field and/or other techniques is needed to ensure dNDVI can accurately detect, delimit, and quantify debris flow features. Future studies should integrate lidar, a tool that is successful in detecting and estimating surficial erosion rates and volumes from channel incisions, interrill and rill erosion (Santi et al., 2008; Wagenbrenner and Robichaud, 2013; Sankey et al., 2017). Future studies also need to track vegetation properties such as types, height, and density, along with the sediment changes, to help refine the interpretation of dNDVI variations (e.g., Omasa et al., 2006; Scheip and Wegmann, 2022). This proposed integration of high-repeat, high-resolution remote sensing methods will provide more reliable data for models in post-fire debris flow emergency assessment.

#### 415 Conclusion

420

425

Estimating changes in post-fire debris flow likelihood in multi-year studies can be challenging with limited resources. Here, we showed that we can track landscape changes during the post-fire recovery period over several years using limited field sampling combined with temporally and spatially high-resolution satellite imagery. This approach allows us access the 2020 Lake Fire post-fire debris flow likelihood in the Los Angeles National Forest. We were able to use field and satellite observation to identify that fast-growing grasses continue to dominate the landscape four years after the fire, and their distribution is largely dependent on precipitation availability. However, our simulations suggest that an increase in vegetation cover does not contribute as significantly as compared to the seasonal variability of hydraulic conductivity. Our measured hydraulic conductivity measurements show an order of magnitude difference between wet and dry conditions even in the fourth year after the fire. Overall, our study shows the complex

https://doi.org/10.5194/egusphere-2025-4671 Preprint. Discussion started: 15 October 2025 © Author(s) 2025. CC BY 4.0 License.



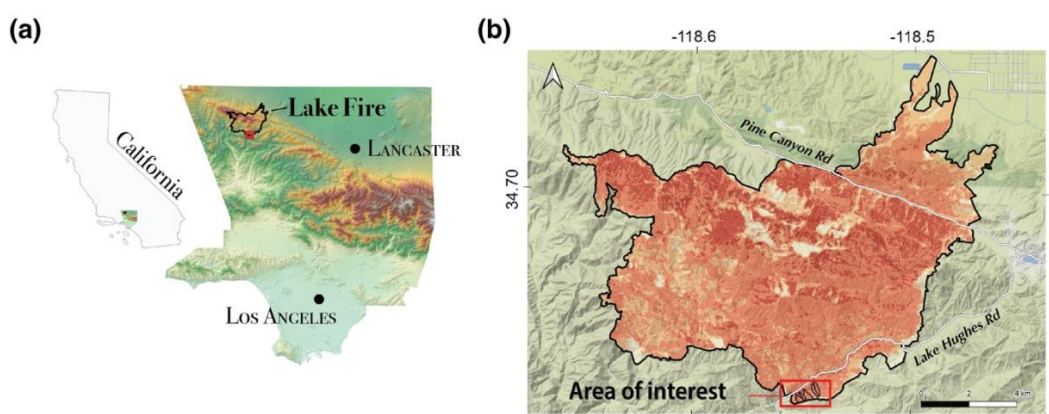


interaction between hydraulic conductivity, grain sizes, and vegetation canopy in contributing to post-fire debris flow likelihood several years after the fire.









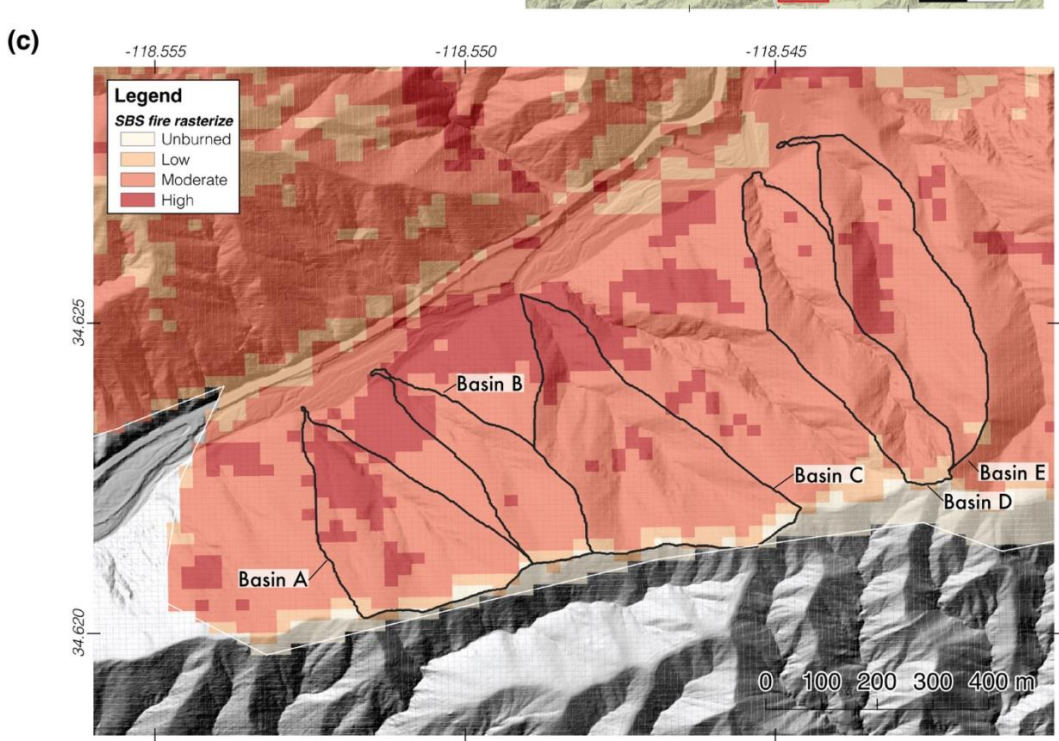
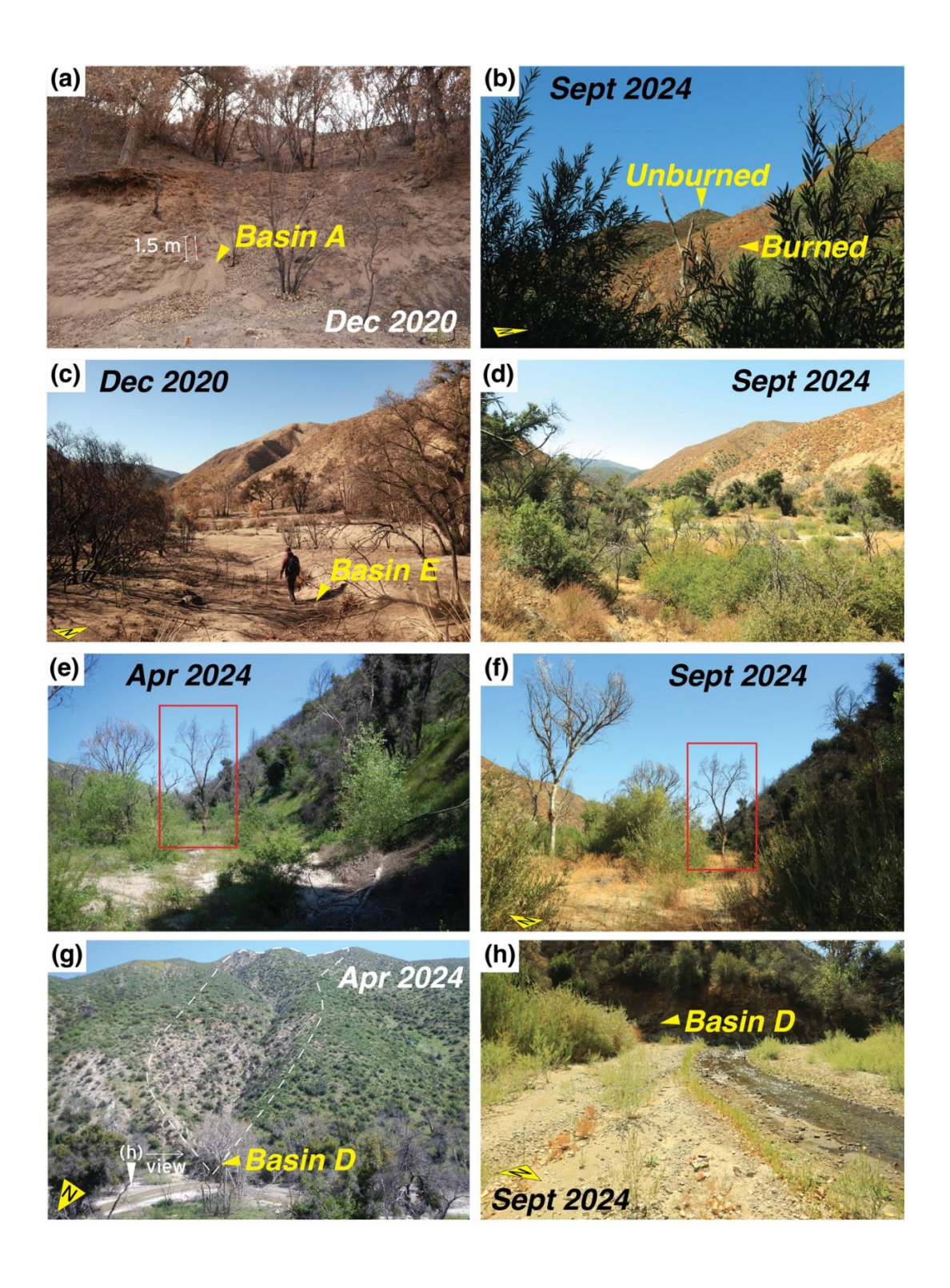


**Figure 1**: (a) General study area location map, (b) The Lake Fire perimeter. Colors represent the different soil burn severity (SBS) from the US Forest Service (US BAER) in (c). The five subbasins used in this study (Black outlined areas). Basin outlets are located at the northern tip of each basin.







https://doi.org/10.5194/egusphere-2025-4671 Preprint. Discussion started: 15 October 2025 © Author(s) 2025. CC BY 4.0 License.



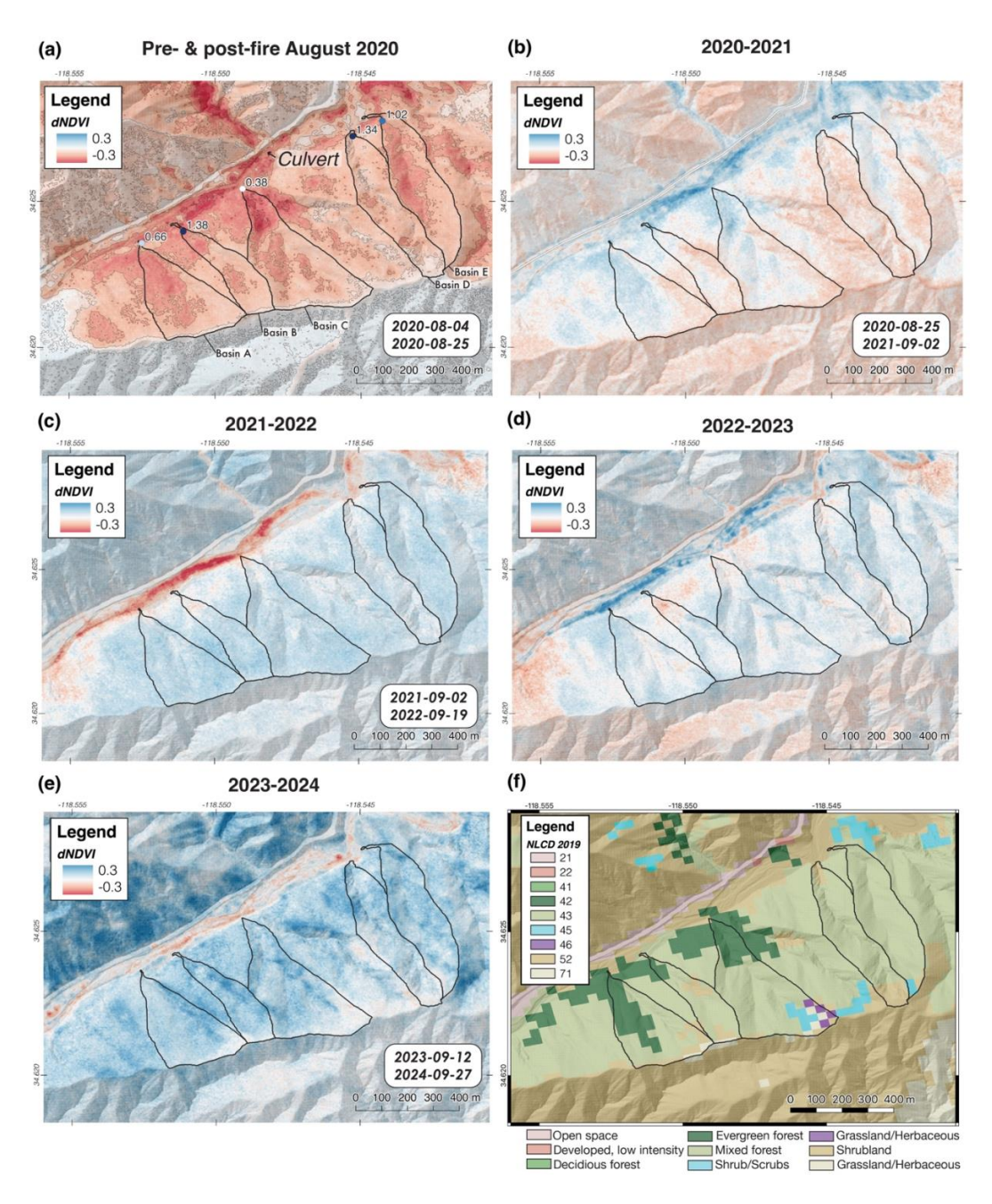


Figure 2: Field comparison of the three field surveys (December 2020, April 2024, and September 2024). (a) Looking NW from Basin E in December 2020. (b) Same as (a) in September 2024. (c) Looking NW towards the vegetation differences between burned and unburned in September 2024. (d) Basin A in December 2020. (e) Looking NE from Basin A to Basin B in April 2024. (f) Same as (e), but in September 2024, the box identifies the same tree as a reference. (g) Looking south at Basin D in April 2024 from the highway. (h) Looking SW at Basin D with the river of lower height in September 2024.

450







**Figure 3**: dNDVI of the study sites (a) changes immediately after the fire, (b-e) the subsequent 4 years, and (f) vegetation classification from NLCD2019 (Yang et al., 2018). Cooler colors indicate an increase in the green index (i.e., vegetation) and warmer colors indicate a loss of the green index (i.e., soil exposure, drying vegetation). The grain sizes of each of the first field surveys are indicated by the circles labeled with the median grain size (d<sub>50</sub>).





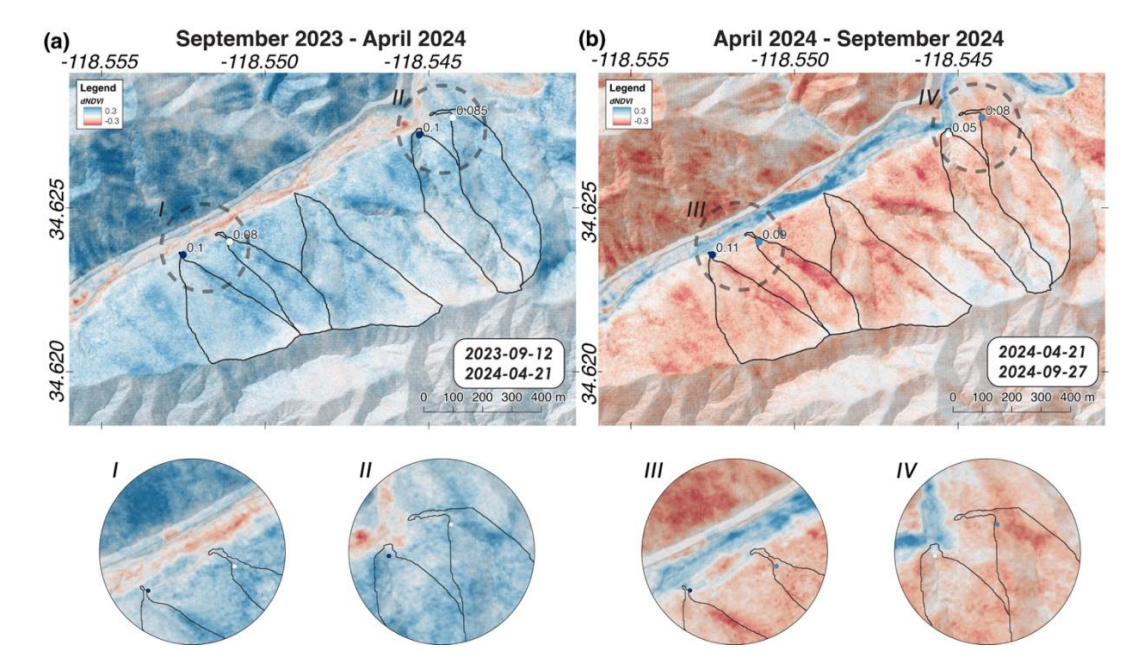


**Figure 4**: dNDVI of the two field surveys (April 2024 and September 2024) post-September 2023. The bottom panel shows a close-up view of the basin outlets. The median grain sizes shown here are listed in **Table 3**.



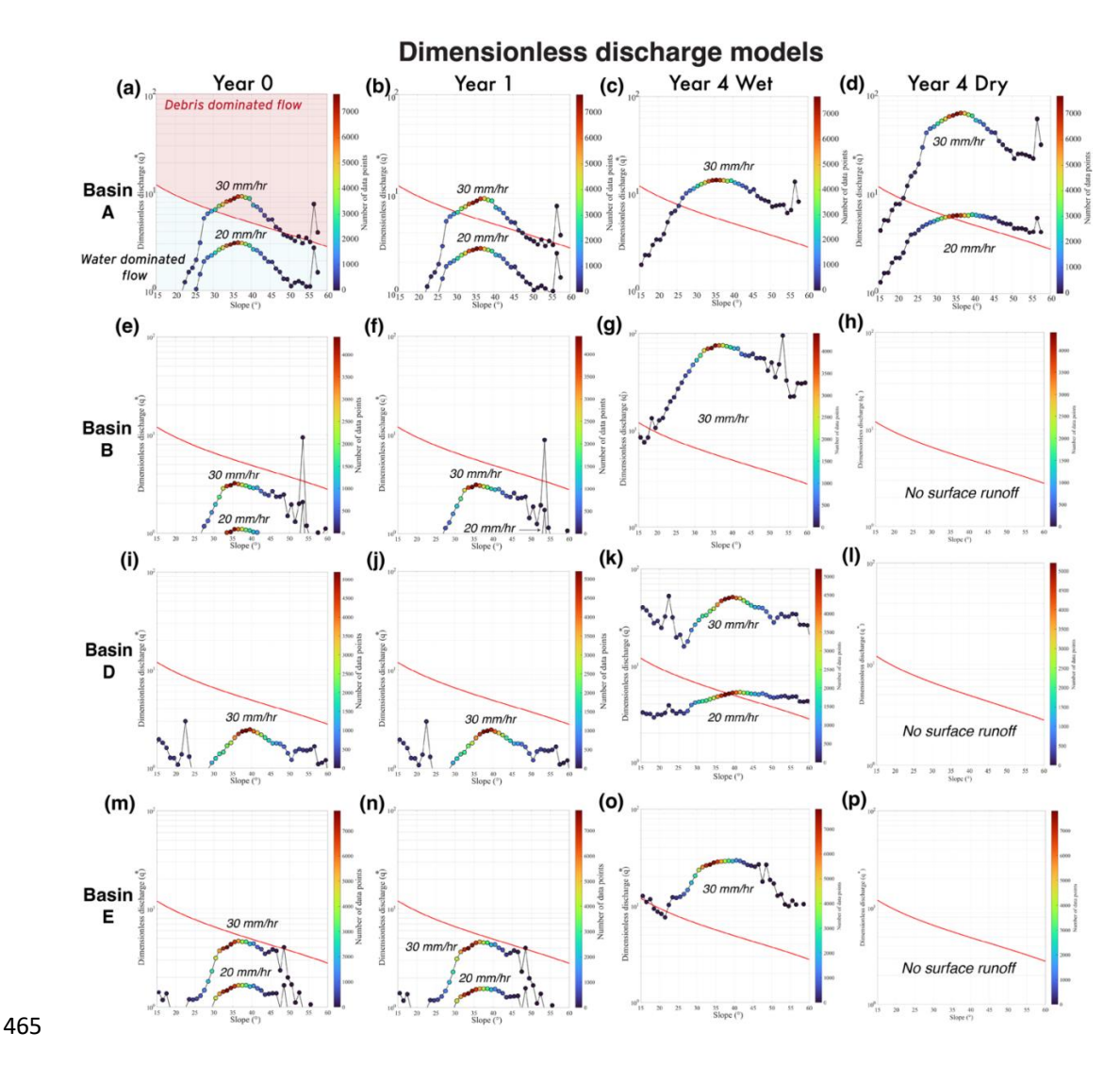


**Figure 5**: Dimensionless discharge models for the 4 basins (A, B, D, E) immediately after fire (Year 0), same soil properties but with full vegetation recovery (Year 1), Year 4 wet and dry seasons. The x-axis represents the slope, and the y-axis represents the dimensionless discharge. Debris-dominated flows, when each slope exceeds the threshold (red line), and water-dominated flows are indicated below the threshold. The rain intensities are in units of mm/hr in a 15-minute rain interval; higher values indicate higher rain intensity.





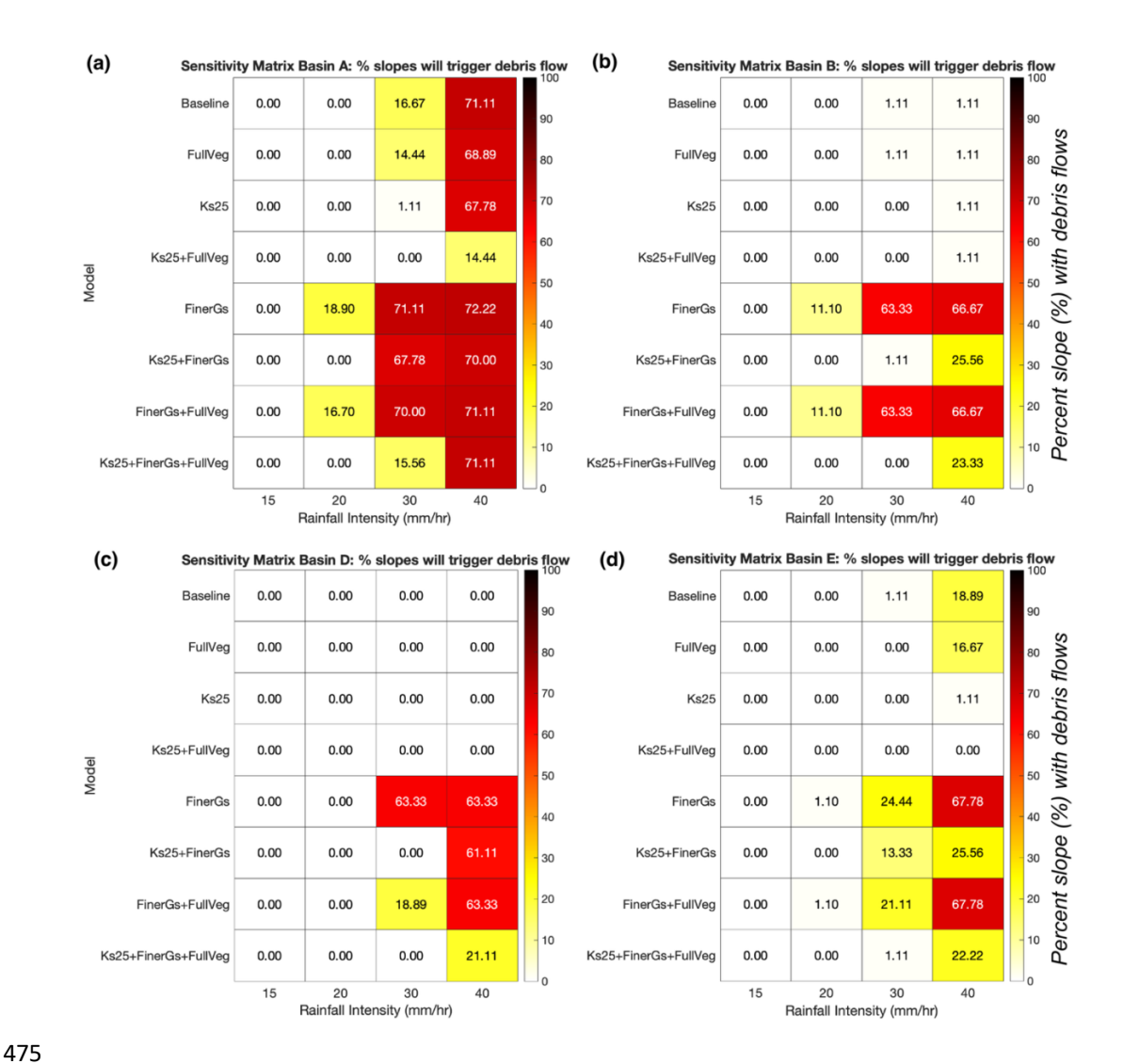


**Figure 6**: Sensitivity test for the vegetation cover, grain size, and hydraulic permeability with different rain intensities (I<sub>15</sub>). Warmer colors indicate a higher percentage of slopes (out of 90 degrees) that exceed the threshold for debris flow. Ks25 indicates a hydraulic conductivity of 25 mm/hr, FullVeg indicates 100% vegetation cover, and Finer Grain Size (FinerGs) indicates a reduction of grain size by 50% from the baseline. See **Table 4** for the description of parameters for each model. % are out of 90 slope degrees.





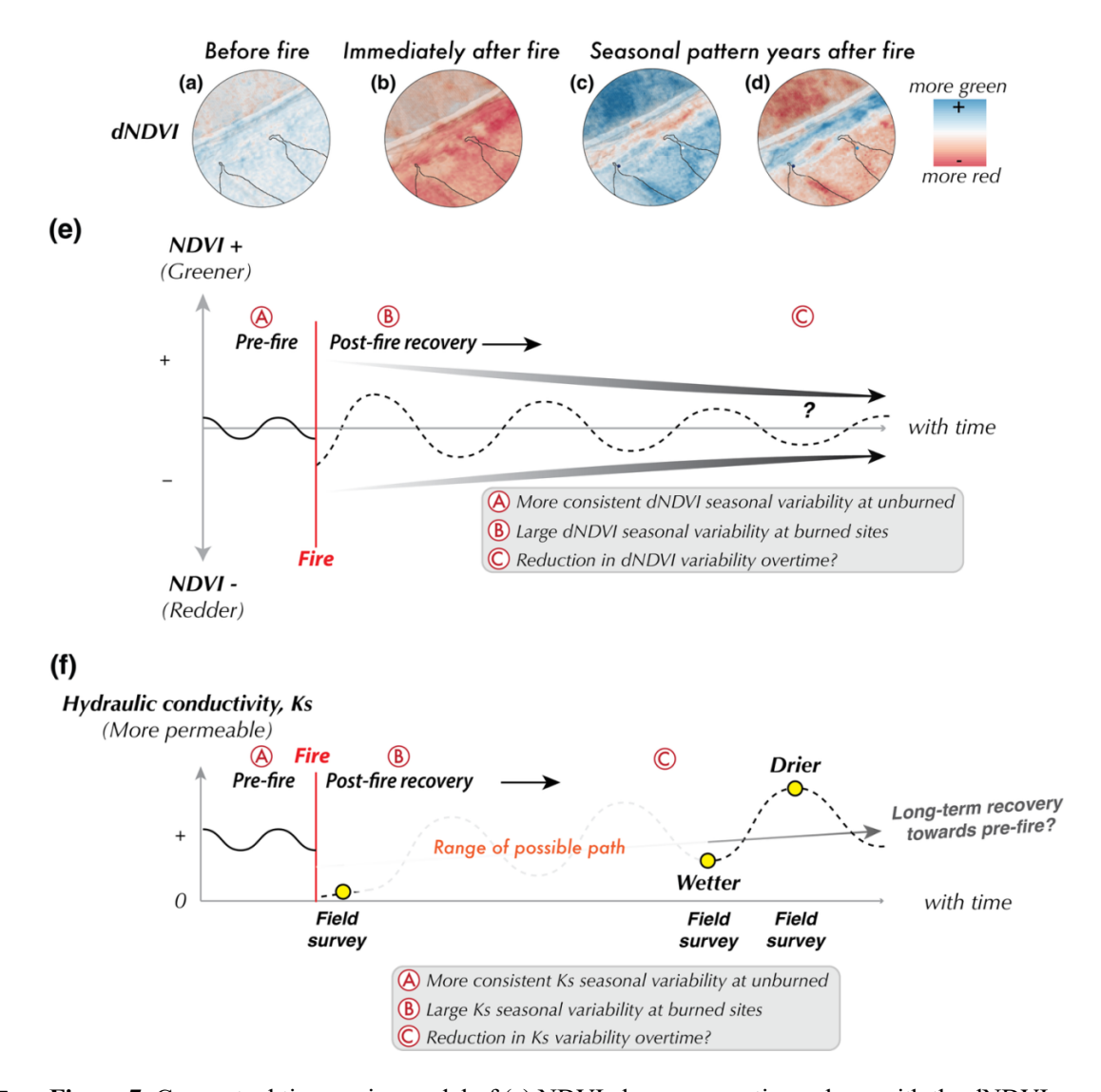


Figure 7: Conceptual time-series model of (a) NDVI changes over time, along with the dNDVI panel above, and (b) proposed non-monotonic hydraulic conductivity changes over time.





#### **Tables**

Year	Predate	Postdate
Pre-Fire	2020-08-06	2020-08-25
1	2020-08-25	2021-09-02
2	2021-09-02	2022-09-19
3	2022-09-19	2023-09-12
4	2023-09-12	2024-09-27
4-Wet	2023-09-12	2024-04-21
4-Dry	2024-04-21	2024-09-27

**Table 1:** The pairs of dNDVI images used to track the yearly vegetation cover and vegetation recovery estimates. Year 4-Wet and Year 4-Dry are defined as the observation period leading up to the field surveys, which also correspond to the seasonal conditions.

S			I			1
Basins	Months since fire	Hydraulic	Vegetation	Pi	<b>d</b> 50	d84
	(MM/YY)	Conductivity	Cover	(Throughfall	(mm)	(mm)
		(mm/hr)	(fraction)	coefficient)		
A	3	$10^{a}$	0	1*	0.66	1.77
	(Dec 2020)					
	12	10 <sup>a</sup>	0.57	0.43	0.66	1.77
	(Sep 2021) 45					
	45	34	0.99	0.01	0.1	0.24
	(Apr 2024) Wet					
	(Apr 2024) Wet 50	22	0.0047	0.99	0.11	0.34
	(Sep 2024) Dry					
В	3	10 <sup>a</sup>	0	1*	1.38	2.45
	(Dec 2020) 12					
	12	10 <sup>a</sup>	0.29	0.71	1.38	2.45
	(Sep 2021) 45					
	45	24	0.99	0.01	0.08	0.26
	(Apr 2024)					
	50	405	0.018	0.99	0.09	0.39
	(Sep 2024)					
С	3	10 <sup>a</sup>	0	1*	0.38	0.9
	(Dec 2020)					
	12	10ª	0.47	0.53	0.38	0.9
	(Sep 2021)					
	(Sep 2021) 45	-	0.98	0.02	-	-
	(Apr 2024)					
	50	-	0.97	0.03	-	-
	(Sep 2024)					
	(Sep 2024)	-	0.054	0.99	-	-
	(Dec 2020)					
D	3	10 <sup>a</sup>	0	1*	1.34	2.45
	(Dec 2020)					
	12	10a	0.03	0.97	1.34	2.45





	(Sep 2021)					
	45	22	0.97	0.03	0.1	0.27
	(Apr 2024)					
	50	576	0.13	0.87	0.05	0.2
	(Sep 2024)					
E	3	10 <sup>a</sup>	0	1*	1.02	1.77
	(Dec 2020)					
	12	10 <sup>a</sup>	0.26	0.74	1.02	1.77
	(Sep 2021)					
	45	31	0.99	0.01	0.085	0.25
	(Apr 2024)					
	50	157	0.049	0.99	0.086	0.32
	(Sep 2024)					

**Table 2**: Input parameters for our dimensionless discharge model over time. dNDVI used for vegetation cover, see the methods section. 45 months later is considered the wet season for Year 4, and 50 months later is considered the dry season for Year 4.

<sup>a</sup> denotes values used from McGuire et al., (2021). We assumed no vegetation cover immediately after the fire (Year 0). Basin C does not have subsequent measurements due to accessibility issues.

Basins	Months since fire (MM/YY)	Debris flow occurrence (slope) in 15 mm/hr	Debris flow occurrence (slope) in 20 mm/hr	Debris flow occurrence (slope) 30 mm/hr
A	3 (Dec 2020)	None	None	>30
	12 (Sep 2021)	None	None	>30
	45 (Apr 2024)	None	None	>26
	50 (Sep 2024)	None	>34	>22
В	3 (Dec 2020)	None	None	None
	12 (Sep 2021)	None	None	None
	45 (Apr 2024)	None	>48	>18
	50 (Sep 2024)	None	None	None
C	3 (Dec 2020)	>55	>30	>27
	12 (Sep 2021)	>57	>33	>29
	45 (Apr 2024)	-	-	-
	50	-	-	-





	(Sep 2024)			
D	3	None	None	None
	(Dec 2020)			
	12	None	None	None
	(Sep 2021)			
	45	None	>38	All
	(Apr 2024)			
	50	None	None	None
	(Sep 2024)			
E	3	None	>50	>45
	(Dec 2020)			
	12	None	None	48 only
	(Sep 2021)			
	45	None	None	>24
	(Apr 2024)			
	50	None	None	None
	(Sep 2024)			

Table 3: Slope thresholds for debris flow initiation at  $I_{15} = 15$ , 20, and 35 mm/hr. Years 0 and 1 have grain size measurements from the first sampling. No vegetation cover for Year 0, and the vegetation cover in Year 1 is from our dNDVI results.

Properties	Vegetation Cover (0 to 1)	Grain Size (ds0) Values from Year 0	Hydraulic Permeability (mm/hr)
Baseline	0	Field measured	10
FullVeg	1	Field measured	10
Ks25	0	Field measured	25
Ks25 + FullVeg	1	Field measured	25
FinerGs	0	50% of the field measured value	10
Ks25 + FinerGs	0	50% of the field measured value	25
FinerGS + FullVeg	1	50% of the field measured value	10
Ks25 + FinerGs + FullVeg	1	50% of the field measured value	25

**Table 4**: Description of the parameters changed for the sensitivity test. The baseline grain sizes are from the first survey in 2020. Simulation results are shown in Figure 6, S5, and S6.



530



#### 515 Code and data availability

The numerical model (KWAVE) used to simulate model runoff can be found through the Community Surface Dynamics Modeling System (CSDMS) model repository at <a href="https://csdms.colorado.edu/wiki/Model:KWAVE">https://csdms.colorado.edu/wiki/Model:KWAVE</a>. The MATLAB codes, results, and descriptions for the models will be available in Chong et al., (2025). The rainfall precipitation record can be obtained from LADPW (<a href="https://dpw.lacounty.gov/wrd/rainfall/">https://dpw.lacounty.gov/wrd/rainfall/</a>). PlanetScope images can be obtained via <a href="https://www.planet.com/explorer/">https://www.planet.com/explorer/</a> through the education and research program.

#### **Author contribution**

Conceptualization: JHC, SH, EL, LS; Data curation: JHC; Formal analysis: JHC; Funding acquisition: JHC; Investigation: JHC, AG, BP, GJ, DB, ML, DU, DS, SH; Methodology: JHC, AG, BP, GJ, DB, ML, DU, DS, SH, LS, EL; Resources: JHC, SH; Software: JHC; Supervision: SH, LS, EL; Visualization: JHC, AG, BP, GJ, DB, ML, DU, DS, SH, EL, LS; Writing (original draft preparation): JHC, AG, BP, GJ, DB, ML, DU, DS, SH, EL, LS; Writing (review and editing).

#### **Competing interests**

The contact author has declared that none of the authors has any competing interests.

#### Disclaimer

Publisher's note: Copernicus Publications remains neutral about jurisdictional claims made in the text, published maps, institutional affiliations, or any other geographical representation in this paper. While Copernicus Publications makes every effort to include appropriate place names, the final responsibility lies with the authors.

#### 540 Acknowledgments

We appreciate the fruitful discussion with Olivia Hoch, Brian Swanson, and Airui Li helped improve the project. A permit from the US Forest Service was obtained for the field sampling.

# **Financial support**

This research is partially funded by the University of New Mexico (UNM) Graduate Professional Student Association grant (2022) awarded to JHC, the UNM Office of Graduate Studies travel grant awarded to JHC, and the 2024 American Society of Photogrammetry and Remote Sensing (ASPRS) William A. Fischer grant awarded to JHC.





#### References

Abatzoglou, J. T. and Williams, A. P.: Impact of anthropogenic climate change on wildfire across western US forests, *Proc. Natl. Acad. Sci. USA*, 113, 11770–11775, https://doi.org/10.1073/pnas.1607171113, 2016.

- Atchley, A. L. and Maxwell, R. M.: Influences of subsurface heterogeneity and vegetation cover on soil moisture, surface temperature and evapotranspiration at hillslope scales, *Hydrogeol. J.*, 19, 289–305, <a href="https://doi.org/10.1007/s10040-010-0690-1">https://doi.org/10.1007/s10040-010-0690-1</a>, 2011
- Bright, B. C., Hudak, A. T., Kennedy, R. E., Braaten, J. D., Khalyani, A. H., et al.: Examining post-fire vegetation recovery with Landsat time series analysis in three western North American forest types, *Fire Ecol.*, 15, 8, https://doi.org/10.1186/s42408-018-0021-9, 2019.
- Cannon, S.H., Bigio, E.R., and Mine, E.: A process for fire-related debris flow initiation, Cerro Grande fire, New Mexico, *Hydrological Processes*, 15, 3011-3023, <a href="https://doi:10.1002/hyp.388">https://doi:10.1002/hyp.388</a>, 2001
- Cannon, S. H., Gartner, J. E., Wilson, R. C., Bowers, J. C., and Laber, J. L.: Storm rainfall conditions for floods and debris flows from recently burned areas in southwestern Colorado and southern California, *Geomorphology*, 96, 250–269, <a href="https://doi.org/10.1016/j.geomorph.2007.03.019">https://doi.org/10.1016/j.geomorph.2007.03.019</a>, 2008.
  - Caine, N.: The rainfall intensity—duration control of shallow landslides and debris flows, *Geogr. Ann. Ser. A Phys. Geogr.*, 62, 23–27, <a href="https://doi.org/10.1080/04353676.1980.11879996">https://doi.org/10.1080/04353676.1980.11879996</a>, 1980.
- Carsel, R. F. and Parrish, R. S.: Developing joint probability distributions of soil water retention characteristics, *Water Resour. Res.*, 24, 755-769, <a href="https://doi.org/10.1029/WR024i005p00755">https://doi.org/10.1029/WR024i005p00755</a>, 1988
  - Chong, J-H., Ghost, A., Page, B., Jesmok, G., Berg, D., Lopez, M., Upadhyay, D., Stone, D., Hauswirth, S., Lindsey, E., and Scuderi, L.: Seasonal influence on Post-Fire Debris Flow likelihood on the 2020 Lake Fire, *Dryad* [Dataset], <a href="https://doi:10.5061/dryad.vdncjsz6t">https://doi:10.5061/dryad.vdncjsz6t</a>, 2025.
- DeGraff, J.V., Cannon, S.H., Gartner, J.E.: The Timing of Susceptibility to Post-Fire Debris Flows in the Western United States, *Environmental & Engineering Geoscience*, 21 (4):, 277–292, <a href="https://doi.org/10.2113/gseegeosci.21.4.277">https://doi.org/10.2113/gseegeosci.21.4.277</a>, 2015.
- Ebel, B.A., and Martin, D.A.: Meta-analysis of field-saturated hydraulic conductivity recovery following wildland fire: Applications for hydrologic model parameterization and resilience assessment, *Hydrological Processes*, 31(21), 3682-2696, <a href="https://onlinelibrary.wiley.com/doi/10.1002/hyp.11288">https://onlinelibrary.wiley.com/doi/10.1002/hyp.11288</a>, 2017
- Ebel, B. A., Wagenbrenner, J. W., Kinoshita, A. M., and Bladon, K. D.: Hydrologic recovery after wildfire: A framework of approaches, metrics, criteria, trajectories, and timescales, *J. Hydrol. Hydromech.*, 70, 412–427, <a href="https://doi.org/10.2478/johh-2022-0033">https://doi.org/10.2478/johh-2022-0033</a>, 2022.



600

605

610

625

630

635



Garber, A.P., Thomas, M. A., and Kean, J.W.: How Long Do Runoff-Generated Debris-Flow Hazards Persist After Wildfire?, *Geophysical Research Letters*, 50(19), https://doi.org/10.1029/2023GL105101, 2023.

Granged, A. J. P., Zavala, L. M., Jordán, A., and Bárcenas-Moreno, G.: Post-fire evolution of soil properties and vegetation cover in a Mediterranean heathland after experimental burning: A 3-year study, *Geoderma*, 164, 85–94, https://doi.org/10.1016/j.geoderma.2011.05.017, 2011.

Gorr, A. N., McGuire, L. A., Beers, R., Youberg, A., Rengers, F. K., Kean, J. W., and Staley, D. M.: Triggering conditions, runout, and downstream impacts of debris flows following the 2021 Flag Fire, Arizona, USA, *Nat. Hazards*, 117, 2473–2504, <a href="https://doi.org/10.1007/s11069-023-05952-9">https://doi.org/10.1007/s11069-023-05952-9</a>, 2023.

Gorr, A. N., McGuire, L. A., Youberg, A. M., Beers, R., and Liu, T.: Inundation and flow properties of a runoff-generated debris flow following successive high-severity wildfires in northern Arizona, USA, *Earth Surf. Process. Landf.*, 49, 622–641, https://doi.org/10.1002/esp.5724, 2024.

Hoch, O.J., McGuire, L.A., Youberg, A.M., and Rengers, F.K.: Hydrogeomorphic Recovery and Temporal Changes in Rainfall Thresholds for Debris Flows Following Wildfire, *Journal of Geophysical Research: Earth Surface*, 126(12), <a href="https://doi.org/10.1029/2021JF006374">https://doi.org/10.1029/2021JF006374</a>, 2021.

Horn, K. J. and St. Clair, S. B.: Wildfire and exotic grass invasion alter plant productivity in response to climate variability in the Mojave Desert, *Landsc. Ecol.*, 32, 635–646, <a href="https://doi.org/10.1007/s10980-016-0466-7">https://doi.org/10.1007/s10980-016-0466-7</a>, 2017.

Iverson, R. M., Logan, M., LaHusen, R. G., and Berti, M.: The perfect debris flow? Aggregated results from 28 large-scale experiments, *J. Geophys. Res.-Earth Surf.*, 115, F03005, https://doi.org/10.1029/2009JF001514, 2010.

Kean, J. W., Staley, D. M., and Cannon, S. H.: In situ measurements of post-fire debris flows in southern California: Comparisons of the timing and magnitude of 24 debris-flow events with rainfall and soil moisture conditions, *J. Geophys. Res.-Earth Surf.*, 116, e2011JF002005, <a href="https://doi.org/10.1029/2011JF002005">https://doi.org/10.1029/2011JF002005</a>, 2011.

Kean, J. W., McGuire, L. A., Rengers, F. K., Smith, J. B., and Staley, D. M.: Amplification of post-wildfire peak flow by debris, *Geophys. Res. Lett.*, 43, 8545–8553, https://doi.org/10.1002/2016GL069661, 2016

Kean, J. W., Staley, D. M., Lancaster, J. T., Rengers, F. K., Swanson, B. J., Coe, J. A., Hernandez, J. L., Sigman, A. J., Allstadt, K. E., and Lindsay, D. N.: Inundation, flow dynamics, and damage in the 9 January 2018 Montecito debris-flow event, California, USA: Opportunities and challenges for post-wildfire risk assessment, *Geosphere*, 15, 1140–1163, https://doi.org/10.1130/GES02048.1, 2019.





- Martinez, J.R., McGuire, L.A., and Youberg, A.M.: Insights into temporal changes in debris flow susceptibility following fire in the Southwest USA from monitoring and repeat estimates of soil hydraulic and physical properties, *Earth Surf. Process. Landforms*, 50, https://doi.org/10.1002/esp.70015, 2025
- McGuire, L.A., and Youberg, A.M.: Impacts of successive wildfire on soil hydraulic properties: Implications for debris flow hazards and system resilience, *Earth Surf. Process. Landforms*, 44, 2236–2250, https://doi.org/10.1002/esp.4632, 2019.
- McGuire, L. A., Rengers, F. K., Oakley, N., Kean, J. W., Staley, D. M., Tang, H., de Orla-Barile, M., and Youberg, A. M.: Time since burning and rainfall characteristics impact post-fire debrisflow initiation and magnitude, *Environ. Eng. Geosci.*, 27, 43–56, <a href="https://doi.org/10.2113/EEG-D-20-00029">https://doi.org/10.2113/EEG-D-20-00029</a>, 2021a.
- McGuire, L. A., Youberg, A. M., Rengers, F. K., Abramson, N. S., Ganesh, I., Gorr, A. N., Hoch, O., Johnson, J. C., Lamom, P., Prescott, A. B., Zanetell, J., and Fenerty, B.: Extreme precipitation across adjacent burned and unburned watersheds reveals impacts of low-severity wildfire on debris-flow processes, *J. Geophys. Res.-Earth Surf.*, 126, e2020JF005997, https://doi.org/10.1029/2020JF005997, 2021b.
- McGuire, L. A., Rengers, F. K., Youberg, A. M., Gorr, A. N., Hoch, O. J., Beers, R., and Porter, R.: Characteristics of debris-flow-prone watersheds and debris-flow-triggering rainstorms
  following the Tadpole Fire, New Mexico, USA, *Nat. Hazards Earth Syst. Sci.*, 24, 1357–1379, <a href="https://doi.org/10.5194/nhess-24-1357-2024">https://doi.org/10.5194/nhess-24-1357-2024</a>, 2024.
- McGuire, L. A., Ebel, B. A., Rengers, F. K., Vieira, D. C. S., and Nyman, P.: Fire effects on geomorphic processes, *Nat. Rev. Earth Environ.*, 5, 486–503, <a href="https://doi.org/10.1038/s43017-024-00557-7">https://doi.org/10.1038/s43017-024-00557-7</a>, 2024.
  - Miller, J. D. and Thode, A. E.: Quantifying burn severity in a heterogeneous landscape with a relative version of the delta Normalized Burn Ratio (dNBR), *Remote Sens. Environ.*, 109, 66–80, https://doi.org/10.1016/j.rse.2006.12.006, 2007.
  - National Oceanic and Atmospheric Administration: Precipitation Frequency Data Server (PFDS), *Hydrometeorological Design Studies Center, Office of Water Prediction*. <a href="https://hdsc.nws.noaa.gov/pfds/pfds">https://hdsc.nws.noaa.gov/pfds/pfds</a> map cont.html?bkmrk=ca. Accessed July 15, 2025
- Nyman, P., Sheridan, G. J., Smith, H. G., and Lane, P. N. J.: Modeling the effects of surface storage, macropore flow, and water repellency on infiltration after wildfire, *J. Hydrol.*, 513, 301–313, https://doi.org/10.1016/j.jhydrol.2014.02.044, 2014.
- Omasa, K., Hosoi, F., and Konishi, A.: 3D lidar imaging for detecting and understanding plant responses and canopy structure, *J. Exp. Bot.*, 58, 881–898, <a href="https://doi.org/10.1093/jxb/erl142">https://doi.org/10.1093/jxb/erl142</a> 2007.





- Perkins, J. P., Diaz, C., Corbett, S. C., Cerovski-Darriau, C., Stock, J. D., Prancevic, J. P., Micheli, E., and Jasperse, J.: Multi-stage soil-hydraulic recovery and limited ravel accumulations following the 2017 Nuns and Tubbs wildfires in northern California, *J. Geophys. Res.-Earth Surf.*, 127, e2022JF006591, https://doi.org/10.1029/2022JF006591, 2022.
  - QGIS.org, QGIS Geographic Information System, QGIS Association, [Computer software] http://www.qgis.org, 2024
- Rengers, F. K., McGuire, L. A., Coe, J. A., Kean, J. W., Baum, R. L., Staley, D. M., and Godt, J. W.: The influence of vegetation on debris-flow initiation during extreme rainfall in the northern Colorado Front Range, *Geology*, 44, 823–826, <a href="https://doi.org/10.1130/G38096.1">https://doi.org/10.1130/G38096.1</a>, 2016a.
- Rengers, F. K., McGuire, L. A., Kean, J. W., Staley, D. M., and Hobley, D. E. J.: Model simulations of flood and debris flow timing in steep catchments after wildfire, *Water Resour. Res.*, 52, 6041–6061, <a href="https://doi.org/10.1002/2015WR018176">https://doi.org/10.1002/2015WR018176</a>, 2016b.
- Rengers, F.K., McGuire, L.A., Kean, J.W., Staley, D.M., ad Youberg, A.M.: Progress in simplifying hydrologic model parameterization for broad applications to post-wildfire flooding and debris-flow hazards, *Journal of Geophysical Research: Earth Surface*, 121(3), 588-608, <a href="https://doi.org/10.1002/esp.4697">https://doi.org/10.1002/esp.4697</a>, 2019
- Rutter, A. J., Morton, A. J., & Robins, P. C.: A predictive model of rainfall interception in forests.

  II. Generalization of the model and comparison with observations in some coniferous and hardwood stands, *Journal of Applied Ecology*, 12(1), 367–380. <a href="https://doi.org/10.2307/2401739.">https://doi.org/10.2307/2401739.</a>
  1975.
- Sankey, J. B., Kreitler, J., Hawbaker, T. J., McVay, J. L., Miller, M. E., Mueller, E. R., Vaillant, N. M., Lowe, S. E., and Sankey, T. T.: Climate, wildfire, and erosion ensemble foretells more sediment in western USA watersheds, *Geophys. Res. Lett.*, 44, 11,520–11,530, https://doi.org/10.1002/2017GL073979, 2017.
- Santi, P. M., deWolfe, V. G., Higgins, J. D., Cannon, S. H., and Gartner, J. E.: Sources of debris flow material in burned areas, *Geomorphology*, 96, 310–321, <a href="https://doi.org/10.1016/j.geomorph.2007.02.022">https://doi.org/10.1016/j.geomorph.2007.02.022</a>, 2008.
- Scheip, C. and Wegmann, K.: Insights on the growth and mobility of debris flows from repeat high-resolution lidar, *Landslides*, 19, 1297–1319, <a href="https://doi.org/10.1007/s10346-022-01862-2">https://doi.org/10.1007/s10346-022-01862-2</a>, 2022.
  - Staley, D. M., Kean, J. W., Cannon, S. H., Schmidt, K. M., Laber, J. L., et al.: Objective definition of rainfall intensity—duration thresholds for the initiation of post-fire debris flows in southern California, *Landslides*, 10, 547–562, <a href="https://doi.org/10.1007/s10346-012-0341-9">https://doi.org/10.1007/s10346-012-0341-9</a>, 2013.
  - Staley, D. M., Negri, J. A., Kean, J. W., Laber, J. L., Tillery, A. C., and Youberg, A. M.: Prediction of spatially explicit rainfall intensity—duration thresholds for post-fire debris-flow generation in



760



the Western United States, *Geomorphology*, 278, 149–162, <a href="https://doi.org/10.1016/j.geomorph.2016.10.019">https://doi.org/10.1016/j.geomorph.2016.10.019</a>, 2017

- Staley, D. M., Kean, J. W., and Rengers, F. K.: The recurrence interval of post-fire debris-flow generating rainfall in the southwestern United States, *Geomorphology*, 370, 107392, https://doi.org/10.1016/j.geomorph.2020.107392, 2020.
- Tang, H., McGuire, L. A., Rengers, F. K., Kean, J. W., Staley, D. M., and Smith, J. B.: Developing and testing physically based triggering thresholds for runoff-generated debris flows, *Geophys. Res. Lett.*, 46, 8830-8839, https://doi.org/10.1029/2019GL083623, 2019a
- Tang, H., McGuire, L. A., Rengers, F. K., Kean, J. W., Staley, D. M., and Smith, J. B.: Evolution of debris-flow initiation mechanisms and sediment sources during a sequence of post-wildfire rainstorms, J. *Geophys. Res.-Earth Surf.*, 124, 1572–1595, <a href="https://doi.org/10.1029/2018JF004837">https://doi.org/10.1029/2018JF004837</a>, 2019b
- Thomas, M. A., Rengers, F. K., Kean, J. W., McGuire, L. A., Staley, D. M., Barnhart, K. R., and Ebel, B. A.: Postwildfire soil-hydraulic recovery and the persistence of debris flow hazards, *J. Geophys. Res.-Earth Surf.*, 126, e2021JF006091, <a href="https://doi.org/10.1029/2021JF006091">https://doi.org/10.1029/2021JF006091</a>, 2021
- Thomas, M. A., Lindsay, D. N., Cavagnaro, D. B., Kean, J. W., McCoy, S. W., and Graber, A. P.: The rainfall intensity–duration control of debris flows after wildfire, *Geophys. Res. Lett.*, 50, e2023GL103645, <a href="https://doi.org/10.1029/2023GL103645">https://doi.org/10.1029/2023GL103645</a>, 2023.
  - Underwood, E. C., Hollander, A. D., Molinari, N. A., Larios, L., and Safford, H. D.: Identifying priorities for post-fire restoration in California chaparral shrublands, *Restor. Ecol.*, 30, e13513, <a href="https://doi.org/10.1111/rec.13513">https://doi.org/10.1111/rec.13513</a>, 2021.
  - USDA Forest Service, Geospatial Technology and Applications Center, BAER Imagery Support Program: Burned Area Reflectance Classification (BARC) Data Bundle for the LAKE Fire occurring on the Angeles National Forest 2020, raster digital data, USDA Forest Service, <a href="https://activefiremaps.fs.fed.us/baer/download.php?year=2020">https://activefiremaps.fs.fed.us/baer/download.php?year=2020</a>, last accessed 27 August 2020.
  - U.S. Geological Survey Landslide Hazards Program: Post-fire debris-flow hazards dashboard, accessed December 2021, <a href="https://landslides.usgs.gov/hazards/postfire\_debrisflow/">https://landslides.usgs.gov/hazards/postfire\_debrisflow/</a>
- Valencia, F.N., Swanson, B.J., and Hernandez, J.L.: Preliminary geologic map of the Burnt Peak 7.5' Quadrangle, Los Angeles County, California: California Geological Survey Preliminary Geologic Map 22-06, scale 1:24,000, 2022.
- Wagenbrenner, J. W. and Robichaud, P. R.: Post-fire bedload sediment delivery across spatial scales in the interior western United States, *Earth Surf. Process. Landforms*, 39, 865–876, <a href="https://doi.org/10.1002/esp.3488">https://doi.org/10.1002/esp.3488</a>, 2014.
  - Yang, L., Jin, S., Danielson, P., Homer, C., Gass, L., Bender, S. M., Case, A., Costello, C., Dewitz, J., Fry, J., Funk, M., Granneman, B., Liknes, G. C., Rigge, M., and others: A new

https://doi.org/10.5194/egusphere-2025-4671 Preprint. Discussion started: 15 October 2025 © Author(s) 2025. CC BY 4.0 License.





- generation of the United States National Land Cover Database: Requirements, research priorities, design, and implementation strategies, *ISPRS J. Photogramm. Remote Sens.*, 146, 108–123, https://doi.org/10.1016/j.isprsjprs.2018.09.006, 2018.
  - Zhang, L., Dawes, W. R., and Walker, G. R.: Response of mean annual evapotranspiration to vegetation changes at catchment scale, *Water Resour. Res.*, 37, 701–708,
- 780 https://doi.org/10.1029/2000WR900325, 2001
  - Zhao, B., Zhang, L., Xia, Z., Xu, W., Xia, L., Liang, Y., and Xia, D.: Effects of rainfall intensity and vegetation cover on erosion characteristics of a soil containing rock fragments slope, *Adv. Civ. Eng.*, 7043428, <a href="https://doi.org/10.1155/2019/7043428">https://doi.org/10.1155/2019/7043428</a>, 2019.